A Method for the Characterization of the Interior of Pits From Single Spaceborne SAR Images

Leonardo Carrer, *Senior Member, IEEE*, Davide Castelletti, Riccardo Pozzobon, Francesco Sauro, and Lorenzo Bruzzone, *Fellow, IEEE*

***Abstract*— Pits are depressions in the ground that occur due to the collapse of the surface layer. The characterization from the orbit of their internal structure using optical images is challenging due to uncontrolled illumination geometry. In this letter, we propose a methodology for the characterization of pits' interiors by exploiting Synthetic Aperture Radar (SAR) images. The methodology analyzes the amplitude and range of the radar echoes originating from the pit's interior to determine its geometric characteristics through data inversion. The experimental results demonstrate that a set of bright reflections in the radar image can be attributed to the response of pits' vertical walls and floor. By applying the proposed methodology and interpreting the radar reflections, we are able to derive a geometric characterization (e.g., depth) of a given pit. The retrieved geometric parameters from SAR data of a terrestrial pit denoted as *Well of Barhout* align well with the ground truth. The findings of this study have implications for both Earth observation and planetary exploration.**

***Index Terms*— Capella space, pit, planetary surfaces, synthetic aperture radar (SAR).**

I. Introduction

PITS and caves are significant targets for terrestrial and planetary exploration. On Earth, they are among the few unexplored environments left. Similarly, cave systems are believed to exist on other celestial bodies, such as Mars [1] and the Moon [2], as indicated by surface collapses known as skylights. These skylights could potentially offer access to underground cave systems. Extracting information about the pit interior using remote sensing data is crucial in this context. However, traditional optical imaging techniques relying on photoclinometry techniques face challenges due to uncontrolled illumination conditions.

Recent research [3] demonstrates that spaceborne Synthetic Aperture Radar (SAR) X-band images can help determine cave characteristics and assess their accessibility near skylights. Radar waves illuminate the regions of interest and are reflected by the cave interior due to the side-looking acquisition geometry of the sensor. It has been shown that radar responses from karstic sinkholes and lava tubes appear as bright signatures in SAR images. However, despite [3] provides a general framework for understanding these signatures, further investigations are required to: 1) understand the properties of the radar response of pits and 2) translate radar observations into measurable 3-D geometric parameters of the pits. As pits are also found on Venus [4], their radar characterization is of interest for the upcoming missions like EnVision [5] that is equipped with an SAR imaging systems operating in S-band.

This letter explores the feasibility of deriving geometric characterizations of terrestrial circular pits using single X-band Very High-Resolution Spaceborne SAR images. The focus on circular pits is motivated by their prevalence in volcanic and karstic terrains on Earth, as well as their expected presence on Mars and the Moon [1], [2].

The letter presents a theoretical model to translate radar observables into pit geometric parameters and utilizes synthetic and real data acquired with the Capella X-band SAR [6] to test the proposed methodology. Multiple single images are combined to obtain a 3-D reconstruction of the pit interior.

The letter is organized as follows. Section II outlines the proposed methodology. Section III presents experimental results based on synthetic data and real acquisitions. Finally, Section IV discusses the conclusion drawn from this work.

II. Proposed Methodology

Let us consider a scenario where a spaceborne SAR system illuminates a circular pit target with a look angle θ_L. The pit is characterized by a diameter D and features internal walls and a cave with heights denoted as H_1 and H_2, respectively [see Fig. 1(a)]. To detect the reflections from the pit's internal walls and floor in the radar image, their backscattering coefficient must exceed that of the surface reflections originating from the same slant range. Typically, these reflections manifest as bright anomalies in the radar image, which are distinct from the rest of the scene being imaged [3]. The pit floor is illuminated by the radar waves when the following condition is satisfied:

$$\theta_L \leq \arctan\left(\frac{D}{H_1}\right). \tag{1}$$

If the condition stated in (1) is not met, only the reflections from the pit's internal walls will be present in the radar image.

Manuscript received 27 February 2024; accepted 26 March 2024. Date of publication 29 March 2024; date of current version 10 April 2024. This work was supported in part by the Italian Space Agency under Contract 2022-23-HH.0 and in part by "Attività scientifiche per il radar sounder di EnVision fase B1" under Grant CUP: F63C22000650005. *(Corresponding author: Lorenzo Bruzzone.)*

Leonardo Carrer and Lorenzo Bruzzone are with the Department of Information Engineering and Computer Science, University of Trento, 38122 Trento, Italy (e-mail: lorenzo.bruzzone@unitn.it).

Davide Castelletti is with Capella Space Corporation, San Francisco, CA 94110 USA.

Riccardo Pozzobon is with the Department of Geosciences, University of Padua, 35122 Padua, Italy, and also with the Istituto Nazionale di Astrofisica-Osservatorio Astronomico di Padova (INAF-OAPD), 35122 Padua, Italy.

Francesco Sauro is with La Venta Geographic Exploration APS, 31100 Treviso, Italy.

Digital Object Identifier 10.1109/LGRS.2024.3383109

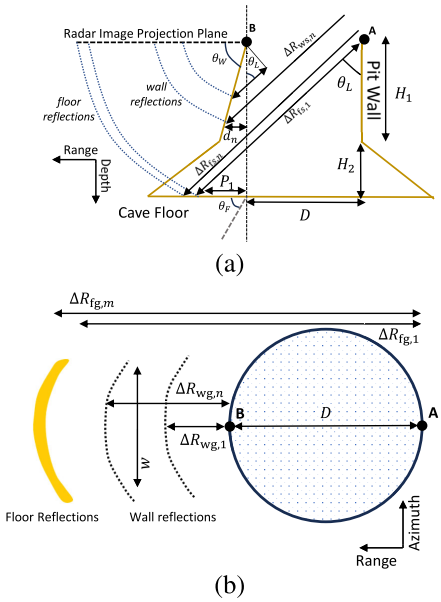

Fig. 1. (a) Pit geometric and radar model (range-depth). (b) Schematic representation of a VHR SAR image of a pit (azimuth-range) along with radar measurable quantities.

Under the assumption that (1) is satisfied, the two primary sets of parameters estimated from the radar image are the ground range intervals of radar reflections originating from specific points on the internal walls and the cave floor. These sets are denoted as $\{\Delta R_{\mathrm{wg},n}\}$ and $\{\Delta R_{\mathrm{fg},m}\}$, respectively [see Fig. 1(b)]. The pedixes wg and fg indicate the range interval relative to the cave wall and floor in ground range coordinates, respectively. Similarly, ws and fs refer to the measurements belonging to the caves' wall and floor in slant range coordinates, respectively. The indexes $n = 1, 2, \ldots, N$ and $m = 1, 2, \ldots, M$ indicate the order of the reflections, where N and M represent the total number of reflections from the cave's internal walls and floor, respectively. The reflections are indexed progressively based on the magnitude of their ground range intervals, from minimum to maximum. The value of $\Delta R_{\mathrm{wg},n}$ is measured with respect to reference point B, while $\Delta R_{\mathrm{fg},m}$ is measured from reference point A. These reference points are located on the edge of the pit, as depicted in Fig. 1. The pit diameter D and the cave width w are directly determined from their ground range interval value on the radar image.

A. Estimation of Cave Floor Parameters

The minimum radar signal propagation inside the pit, denoted as P_1, is equal to

$$P_1 = \Delta R_{\mathrm{fg},1} \sin\theta_I \sin\theta_L - D = \Delta R_{\mathrm{fs},1} \sin\theta_L - D \tag{2}$$

where $\Delta R_{\mathrm{fs},1} = \Delta R_{\mathrm{fg},1} \sin\theta_I$ represents the slant range interval of the response originating from the cave floor, and θ_I is the local incidence angle. The measurement uncertainty of (2), denoted as $\Delta\hat{P}$, is equal to $\Delta\hat{P} = R_r \sin\theta_I \sin\theta_L$, where R_r is the radar ground range resolution.

The slant range interval $\Delta R_{\mathrm{fs},1}$ is equal to

$$\Delta R_{\mathrm{fs},1} = (H_1 + H_2)\sqrt{1 + \tan^2\theta_L}. \tag{3}$$

Based on (3), one can observe that the ground range interval $\Delta R_{\mathrm{fg},m} = \Delta R_{\mathrm{fs},m}/\sin\theta_I$ assumes large values when considering typical terrestrial pit dimensions on the order of tens of meters [7]. Consequently, the radar reflections from the floor appear significantly displaced in the radar image from the pit's reference surface point if $\Delta R_{\mathrm{fg},m}/R_r \gg 1$. This displacement is a distinctive characteristic of pits that is not present in previously analyzed geological features such as lava tubes [3].

Assuming a flat cave floor, the depth of the floor reflections $H = H_1 + H_2$ can be estimated using $\Delta R_{\mathrm{fs},1}$ as follows:

$$\hat{H} = \Delta R_{\mathrm{fs},1} \cos\theta_L. \tag{4}$$

The measurement uncertainty of (4), denoted as $\Delta\hat{H}$, is equal to $\Delta\hat{H} = R_r \sin\theta_I \cos\theta_L$.

The radar signal propagation P_m inside the pit for a given floor reflection is equal to

$$\hat{P}_m = P_1 + \Delta R_{\mathrm{fg},m} - \Delta R_{\mathrm{fg},1}\, m > 1. \tag{5}$$

Under the assumption of a flat floor, the relative error $e_P = (\hat{P}_m - P_m)/P_m$ is given by

$$e_P = \tan\theta_F \cot\theta_L \tag{6}$$

where θ_F represents the floor inclination. The value of e_P is sensitive to changes in floor inclination. Assuming an acceptable value of e_P to be 0.2, the floor inclination should be lower than approximately 5°.

B. Estimation of Pit Wall Parameters

In the assumption of the far-field regime and vertical pit walls, the estimated depth of a specific wall reflection, denoted as $\hat{h}_n \leq H_1$, is given by

$$\hat{h}_n = \frac{\Delta R_{\mathrm{wg},n} \sin\theta_I}{\cos\theta_L} = \frac{\Delta R_{\mathrm{ws},n}}{\cos\theta_L} \tag{7}$$

where $\Delta R_{\mathrm{ws},n} = h_n \cos\theta_L + d_n \sin\theta_L$ represents the slant range difference between the reflections originating from the true depth h_n of the pit wall and the reference point B (see Fig. 1). The variable d represents the horizontal displacement of the wall point from the normal of the cave floor passing through point B. The measurement uncertainty of (7), denoted as $\Delta\hat{h}$, is equal to $\Delta\hat{h} = R_r \sin\theta_I/\cos\theta_L$, where R_r is the radar ground range resolution.

The relative error $e_h = (\hat{h}_n - h_n)/h_n$ in depth estimation resulting from the assumption of vertical wall is given by

$$e_h = \frac{d_n}{h_n}\tan\theta_L = \cot\theta_W \tan\theta_L \tag{8}$$

where $\cot\theta_W = d_n/h_n$ represents the vertical wall inclination or slope for all n. Due to the fractured nature of basaltic rocks, which are a common material for planetary pits, pit walls have vertical or nearly vertical orientations [4]. If we assume $\theta_W > 70°$ for basalt pit walls, this results in an approximation error $e_h < 0.2$ when using (7), which is an acceptable value for practical purposes.

C. Pit Wall and Floor Parameters Combination for 3-D Estimation

The estimated depths of wall reflections $\hat{h}_n$ and the estimated floor reflection depth $\hat{H}$, along with the estimated signal propagation inside the cave $\hat{P}_m$, are combined to create a 3-D representation of the pit's interior. Under the assumption of both nearly-vertical pit walls and flat floor, the pit wall is modeled as a cylinder with diameter D, while the floor is represented as a series of concentric circles with diameter $D + P_m$. The pit reflections are positioned on the SAR image at Cartesian coordinates $(x_{\mathrm{R}}, y_{\mathrm{R}})$ [range, azimuth] from the assumed center of the pit at $(x_0, y_0) = (0, 0)$. The parametric equations of a circle with diameter D are given by $(x_c = D/2\cos\theta, y_c = D/2\sin\theta)$, where $0 \leq \theta < 2\pi$. For each wall reflection, its SAR image position $(x_{\mathrm{R},n}, y_{\mathrm{R},n})$ is translated to the position $(x_{\mathrm{c},n} = D/2\cos\theta_n, y_{\mathrm{c},n} = D/2\sin\theta_n)$, where θ_n is the angle that minimizes the following Euclidean distance from the circle:

$$\theta_n = \min_{\theta}\left\{\sqrt{[x_{\mathrm{R},n} - x_c(\theta)]^2 + [y_{\mathrm{R},n} - y_c(\theta)]^2}\right\}. \quad (9)$$

Each floor reflection is translated using a similar procedure but considering the assumption of $(x_c = D/2\cos\theta + P_m, y_c = D/2\sin\theta + P_m)$ as the parametric equations of the circle. The z component is equal to $\hat{h}_n$ or $\hat{H}$ depending on the type of reflection (i.e., wall or floor).

III. Experimental Results

A. Dataset Description

We present the case study of the *Well of Barhout*, a circular pit located in Yemen that is considered a planetary analog of martian and lunar circular pits. The entrance of the pit has a diameter of $D = 30$ m, while the bottom widens to a diameter of approximately 120 m at the base [8]. This indicates that the maximum radar signal propagation P inside the cave is $(120 - D)/2 = 45$ m. The overall depth of the pit is about $H_1 + H_2 = 112$ m, with the wall height H_1 measuring 61 m. Consequently, the cave height is $H_2 = 51$ m.

To test and validate our methodology we first generated a synthetic 3-D model of the pit (see Section III-B) for conducting 3-D radar simulations. Then, we acquired nine SAR images of the *Well of Barhout* (see Section III-C). The pit was observed from various look directions, resulting in a set of look angles θ_L ranging from approximately 23° to 37°, depending on the image. The images were acquired using Capella's X-band Radar [6] in spotlight mode providing an image resolution of about 0.5 × 0.5 m. In detail, we exploited Capella's GEO data products that are range and azimuth compressed and include multilooking. The images are terrain-height corrected using a high-resolution Digital Elevation Model (DEM) and projected assuming a Universal Transverse Mercator (UTM) projection.

B. Results on 3-D Radar Simulations

Fig. 2(a) illustrates the synthesized 3-D model of the *Well of Barhout*, based on the pit dimensions outlined in Section III-A, with the pit wall modeled after observed layering in optical images. Fig. 2(b) and (c) depict the results of 3-D ray-tracing simulations using Persistence of Vision Raytracer (POV-Ray) on the model from Fig. 2(a), considering various values of θ_L. These simulations reveal that the amount of specular scattering from the pit wall strongly depends on the relative orientation of the wall layering with respect to the look angle, and that floor reflections result in specular scattering. The floor reflections are visible when the condition in (1) is met. For the *Well of Barhout*, this condition corresponds to $\theta_L \leq 26.19°$.

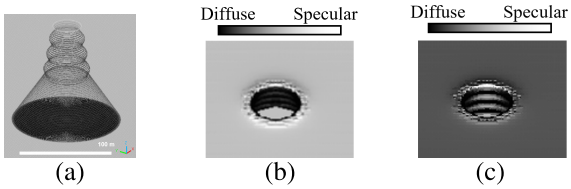

Fig. 2. (a) Three-dimensional model of the *Well of Barhout*. 3-D Ray-tracing simulation showing the amount of diffuse and specular scattering originating from the pit assuming (b) $\theta_L = 25°$ and (c) $\theta_L = 35°$.

Fig. 3 displays the results of 3-D radar simulations conducted on the model presented in Fig. 2(a) for various values of θ_L, performed using RaySAR [9]. The results show that radar reflections from the pit wall appear as narrow semicircular features with increasing intensity for higher values of θ_L, while reflections from the pit floor, visible at look angles of 20° and 25°, are more spatially distributed compared to the wall reflections, with intensity increasing for lower values of θ_L. Ground range values of wall and floor reflections depend on acquisition geometry (see Section II), with floor reflections appearing considerably displaced from the pit position, with a ground range position $\Delta R_{\mathrm{fg},1}$ on the order of 300 m, aligning with theoretical modeling based on the conversion of (3) to ground range, assuming $\theta_I = \theta_L$.

C. Results on Experimental Data

1) Analysis of Radar Reflections: Fig. 4 shows two examples of the acquired Capella X-Band SAR images of the *Well of Barhout* with different look directions. The look angles of the two images are 35.54° [see Fig. 4(a)] and 36.48° [see Fig. 4(b)]. The radar images display several bright semicircular reflections aligned with the radar look direction, resembling the ones observed in the 3-D radar simulations [see Fig. 3(d)]. Accordingly, we can conclude that these reflections originate from the circular walls of the pit. However, no reflections from the cave floor are visible in these images as the look angles for these acquisitions are greater than the floor illumination condition of (1), which is 26.19°.

Fig. 5 presents another pair of X-band SAR images with a similar look direction. The look angles for Fig. 5(a) and (b) are 31.88° and 23.56°, respectively. Fig. 5(a) does not show any features related to the cave floor, as expected based on the look angle of the image. Fig. 5(b) displays an anomalous and distributed reflection located at a significant ground range distance of at least 300 m from the pit edge. This feature is absent in Fig. 5(b). We attribute this reflection to the cave floor based

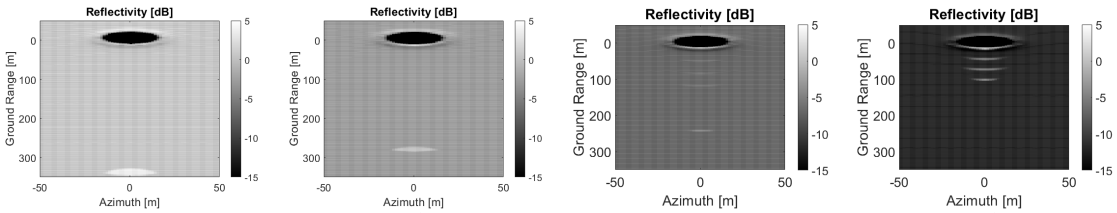

Fig. 3. Three-dimensional radar simulations [9] results for (a) $\theta_L = 20°$, (b) $\theta_L = 25°$, (c) $\theta_L = 30°$, and (d) $\theta_L = 35°$.

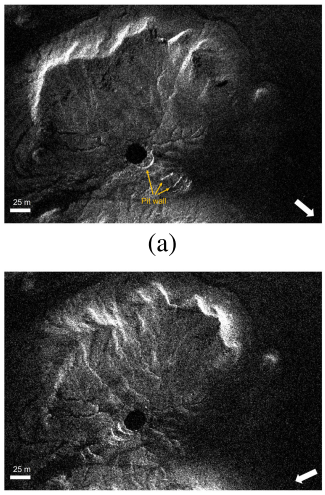

Fig. 4. Analysis of *Well of Barhout*, Yemen. Capella X-band Spaceborne SAR Images with (a) South-East ($\theta_L = 35.54°$) and (b) South-West ($\theta_L = 36.48°$) look direction. Several semicircular reflections originating from the pit walls are visible in the images. The white arrow indicates the radar illumination direction.

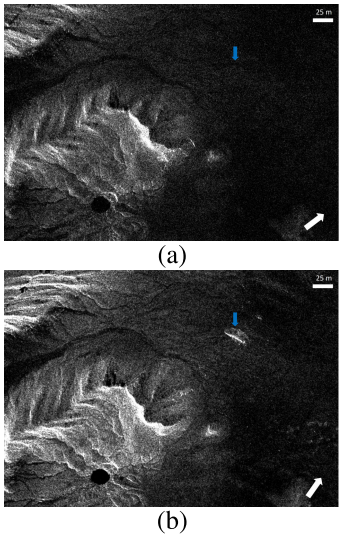

Fig. 5. Analysis of *Well of Barhout*, Yemen. Capella X-band Spaceborne SAR images with (a) $\theta_L = 31.88°$ and (b) $\theta_L = 23.56°$. The two SAR images have a similar acquisition geometry. The white and the blue arrows indicate the radar illumination direction and the position of the floor reflections, respectively.

on its agreement with the simulation results [see Fig. 3(a)] and the ground range interval value of $\Delta R_{\text{fg},1} = 300$ m, which closely matches the theoretical modeling value of 306 m [see ground range conversion of (3)]. The corresponding optical

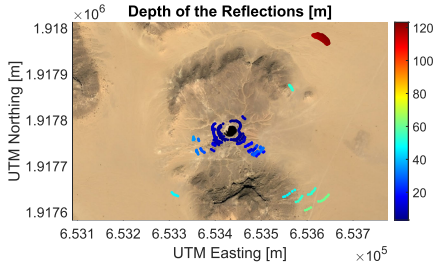

Fig. 6. Identified pit reflections and their estimated depth. The reflections originate either from the pit walls or floor. The detected features are superimposed to the optical image (Bing) of the *Well of Barhout*. The image was obtained by combining the results of nine different SAR images having different look directions.

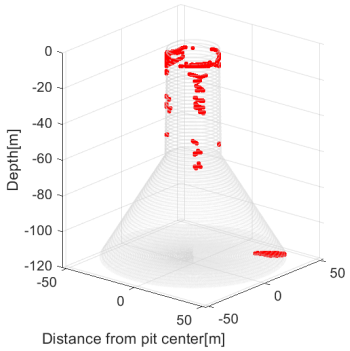

Fig. 7. Three-dimensional reconstruction (shown in red) of the pit vertical walls and floor based on the identified reflections of Fig. 6. The reference model in gray qualitatively illustrates a plausible pit structure coherent with the reconstruction from data.

image captured over the same area does not reveal any surface feature that could explain the anomalous reflections.

2) Pit Parameters Estimation: Fig. 6 illustrates the geographic location and estimated depth of all manually identified pit wall and floor reflections by combining the results of nine images with different look directions. The maximum estimated depth of the wall reflections is 62.1 ± 0.38 m, which exhibits excellent agreement with the in situ survey value of 61 m.

The estimated depth of the floor reflections is 116.45 ± 0.24 m that is consistent with the ground truth value of $H_1 + H_2 = 112$ m. The signal propagation value P inside the cave [see (5)] ranges between 20.8 ± 0.18 m and 37.6 ± 0.18 m, which aligns with the maximum expected value of 45 m. Based on optical evidence of the interior of the pit, the floor inclination θ_F is minimal, allowing the cave to be approximated as flat.

Fig. 7 illustrates the 3-D reconstruction of the pit using the procedure detailed in Section II-C. The image depicts

the wall layering and the relative positioning of the wall and floor reflections. However, the pit reconstruction remains incomplete due to missing parts of the floor and wall response in the data. This incompleteness can be attributed to several factors. As highlighted in the 3-D radar simulations (see Section III-B), the backscattering from the pit wall strongly depends on the relative orientation between the radar illumination direction and the wall layering structure. Consequently, sections of the wall may reflect energy away from the radar, resulting in minimal energy returned to the sensor. Another contributing factor is the lack of radar illumination for certain wall sections due to orbital constraints (e.g., the North wall of the pit). The partial absence of floor reflections can be attributed to the strong surface backscattering response from the pit surroundings, which masks the weaker pit floor reflections occurring at the same slant range. It is worth noting that we were able to detect the floor reflection over a particularly smooth surface area [see Fig. 5(b)].

IV. Discussion and Conclusion

Through 3-D radar simulations and real data analyses, we have demonstrated that natural pit structures exhibit distinct radar signatures in spaceborne SAR images, providing insights into their internal walls and floor. Our theoretical model translates these radar signatures into geometric quantities, such as reflection depth, enabling us to achieve 3-D geometric reconstructions of pits by combining multiple radar images. While our methodology primarily focuses on circular pits, it can be readily adapted to elliptical pits, representing a potential avenue for future investigation.

Traditionally, precise 3-D geometric reconstruction relies on radar techniques like interferometry and stereo radargrammetry. However, by leveraging the unique characteristics of pit radar responses and prior knowledge of pit geometry, we conduct reconstruction without image pairs, ensuring high accuracy. Our analysis estimates the maximum depths of the pit wall and cave floor at 62.1 ± 0.38 m and 116.45 ± 0.24 m, respectively, closely aligning with ground truth values of 61 and 112 m.

Our results reveal that the pit's radar signature can be identified in the SAR image by comparing it with simulations of the pit's 3-D model. If the pit ground truth model is not available, generating a set of SAR simulations using different pit models and finding the best match with experimental data offers a solution for correctly associating radar reflections with the wall and floor. Additionally, if a digital terrain model is available, an accurate simulation of the response from the surface can help ruling out bright features belonging to other targets. In cases of multiple images with varying illumination directions, analyzing the radar response across them can reveal the presence of pit reflections, tracking how the illuminated portion of the pit interior varies from one image to another.

In future research, we aim to: 1) explore 3-D pit characterization using stereo or interferometric image pairs and 2) develop automatic techniques for SAR image feature extraction and 3-D reconstruction of pits. Note that the use of interferometric techniques holds promise for further improving the accuracy of the pit's geometric parameter estimation. However, it also poses challenges due to the inherent superposition between the surface and the pit radar response, affecting the phase of the signal. As a final remark, it is important to point out that our work bears significant implications for planetary exploration, particularly considering the absence of spaceborne SAR systems beyond Earth. With circular pits already identified on Mars, our findings could support advocating for SAR system development in future Mars missions.

Acknowledgment

SAR imagery provided by Capella Space under the Open Data Community program. The authors would like to thank Elena Diana for supporting in analyzing the Well of Barhout images.

References

[1] G. Cushing, "Candidate cave entrances on Mars," *J. Cave Karst Stud.*, vol. 74, no. 1, pp. 33–47, Apr. 2012.
[2] J. Haruyama et al., "Possible lunar lava tube skylight observed by SELENE cameras," *Geophys. Res. Lett.*, vol. 36, no. 21, pp. 1–5, Nov. 2009.
[3] L. Carrer, D. Castelletti, R. Pozzobon, F. Sauro, and L. Bruzzone, "A novel method for hidden natural caves characterization and accessibility assessment from spaceborne VHR SAR images," *IEEE Trans. Geosci. Remote Sens.*, vol. 61, 2023, Art. no. 4500111.
[4] D. Y. Wyrick and D. L. Buczkowski, "Pit Crater chains across the solar system: Evidence for subterranean tectonic caves, porosity and permeability pathways on planetary bodies," *J. Geophys. Res., Planets*, vol. 127, no. 12, Dec. 2022, Art. no. e2022JE007281.
[5] R. C. Ghail, D. Hall, P. J. Mason, R. R. Herrick, L. M. Carter, and E. Williams, "VenSAR on EnVision: Taking Earth observation radar to Venus," *Int. J. Appl. Earth Observ. Geoinf.*, vol. 64, pp. 365–376, Feb. 2018.
[6] D. Castelletti et al., "Capella space VHR SAR constellation: Advanced tasking patterns and future capabilities," in *Proc. IEEE Int. Geosci. Remote Sens. Symp.*, Jul. 2022, pp. 4137–4140.
[7] F. Sauro, R. Pozzobon, M. Massironi, P. De Berardinis, T. Santagata, and J. De Waele, "Lava tubes on Earth, Moon and Mars: A review on their size and morphology revealed by comparative planetology," *Earth-Sci. Rev.*, vol. 209, Oct. 2020, Art. no. 103288.
[8] Well of Barhout. (2010). *Well of Barhout—Wikipedia, the Free Encyclopedia*. Accessed Jun. 23, 2023. [Online]. Available: https://en.wikipedia.org/wiki/Well_of_Barhout
[9] S. Auer, S. Hinz, and R. Bamler, "Ray-tracing simulation techniques for understanding high-resolution SAR images," *IEEE Trans. Geosci. Remote Sens.*, vol. 48, no. 3, pp. 1445–1456, Mar. 2010.

Open Access funding provided by 'Università degli Studi di Trento' within the CRUI CARE Agreement